Hindawi Publishing Corporation
Advances in Materials Science and Engineering
Volume 2016, Article ID 6270129, 7 pages
http://dx.doi.org/10.1155/2016/6270129

Research Article

Oxygen Defect-Mediated Magnetism in Fe-C Codoped TiO_2

Zhaorui Zou,[1,2] Zhongpo Zhou,[1,2,3] Haiying Wang,[1,2] and Meng Du[1,2]

[1]*College of Physics and Material Science, Henan Normal University, Xinxiang 453007, China*
[2]*Henan Key Laboratory of Photovoltaic Materials, Xinxiang 453007, China*
[3]*Key Laboratory of Artificial Micro- and Nanostructures of Ministry of Education and School of Physics and Technology, Wuhan University, Wuhan 430072, China*

Correspondence should be addressed to Zhongpo Zhou; paul@whu.edu.cn and Haiying Wang; wanghaiy@whu.edu.cn

Received 11 June 2016; Revised 15 August 2016; Accepted 24 August 2016

Academic Editor: Pavel Lejcek

The magnetic properties of the C doped and C-Fe codoped TiO_2 films fabricated by sol-gel and spin coating have been investigated combining experiments and first-principles calculations. All the samples exhibit the anatase crystal phase and the room temperature ferromagnetism. The values of the saturation magnetizations are in the order of Fe-C codoped TiO_2 > Fe-C codoped TiO_2 (annealed in O_2) > C doped TiO_2 > C doped TiO_2 (annealed in O_2). The calculated net moment values are in the order of Fe-C codoped TiO_2 > C doped TiO_2 with oxygen vacancies existing, in accord with the experimental results. The hybridization of Fe 3*d*, C 2*p*, and O 2*p* (nearest to the Fe defect) led to the spin split of Fe 3*d*, C 2*p*, and O 2*p* which contributed to the ferromagnetism.

1. Introduction

Diluted magnetic semiconductors (DMSs) are promising candidates for the spin-polarized devices such as magnetooptical, nonvolatile storage and other spin logical devices [1]. However, most of these DMSs have relatively low Curie temperatures (T_C), reducing their practical usefulness. In the recent decades, oxide diluted magnetic semiconductors such as ZnO [2], SnO_2 [3], and TiO_2 [4] doped with magnetic transition metal elements have attracted considerable attention, due to the discovery of room temperature (RT) ferromagnetism (FM) in these systems. Several theoretical investigations have been reported, most of which focus on the cation vacancies in TiO_2 bulk materials [5–10]. However, recent studies showed that the unexpected RT FM is closely related to the oxygen vacancies (Vos) instead of the cation vacancies [11–17]. Vo is a type of defects in TiO_2 which can be manipulated relatively easily during the synthesis processing [17]. Near the surface or in the bulk, Vos can lead to ferromagnetism enabling a possible application for TiO_2 as a magnetic semiconductor in spintronics [18].

In TiO_2 based DMSs, it is concluded that there are four factors related to the observed ferromagnetism: the Vos, cation vacancies, transition metal dopants, and the change of titanium oxidation state (Ti^{3+}) [16]. On the one hand, the Vos can cause an obvious change in the band structure and make a significant contribution to the FM. On the other hand, the transition metal elements which have unpaired d-electrons can provide magnetic moment to the DMSs. In this paper, we have investigated the electronic and magnetic properties of transition metal (Fe), nonmetal C, and Vos codoped anatase TiO_2 ($Ti_{31}FeO_{62}C$) combining the experiments and the first-principles calculations based on the density-functional theory (DFT). The experimental results are consistent with the first-principles calculations. The magnetism induced by the Fe and C (Fe-C) codoping is investigated being associated with the V_O defect electrons. The connections between doped Fe ions, C ions, and Vos are discussed to explain the ferromagnetism observed in these materials.

2. Experiments and Calculations

The C doped TiO_2 films, C doped TiO_2 films (annealed in O_2), Fe-C codoped TiO_2 films, and Fe-C codoped TiO_2 films (annealed in O_2) were prepared by sol-gel and spin-coating methods. A clear solution was prepared by reacting tetrabutyl titanate ($C_{16}H_{36}O_4Ti$) and nanotube carbon (C) with a mixture of water and hydrochloric acid (HCl) in an

ethanol (C_2H_5OH) diluted medium. The C doped TiO_2 films were spin-coated on the fluorine doped tin oxide (FTO) substrates with the mentioned solution. After the prebaking at 70°C for 30 min, these films were annealed at 450°C for 2 h in O_2 gas and in air to obtain the C doped and the Vos-decreased C doped TiO_2 films, respectively. To get the Fe-C codoped samples, iron nitrate hydrate was added into deionized water; and the C doped TiO_2 films were immersed in the solution for 1 hour. Following the same procedure as that for the C doped and the Vos-decreased C doped TiO_2 samples, the Fe-C codoped and the Vos-decreased Fe-C codoped samples were prepared.

The crystal structures were characterized by X-ray diffraction (XRD, Bruker D8 Discover) with Cu Kα radiation (λ = 1.54 Å). The electronic structures were measured by the X-ray photoelectron spectroscopy (XPS) and the binding energy of the XPS spectra was calibrated with reference to the C 1s peak at 284.6 eV. The optical absorption spectra in the wavelength range of 200–800 nm were measured by using ultraviolet-visible near infrared spectrophotometer (CARY5000, Varian) at RT under the diffuse reflection mode with the integrating sphere. The photoluminescence (PL) spectra were conducted by using the 325 nm He–Cd laser (20 MW) as an excitation light source. The magnetic properties were studied using a vibrating-sample magnetometer (VSM) equipped in the physical property measurement system (PPMS, Quantum Deign). The magnetization loops were recorded with the magnetic field from −1 T to 1 T (T is the abbreviation of Tesla) applied parallel to the samples surfaces.

First-principles calculations based on spin-polarized density-functional theory and projector augmented wave (PAW) pseudopotential technique are performed as implemented within the Vienna Ab-Initio Simulation Package (VASP) [19, 20]. The generalized gradient approximation (GGA-PBE) for the wave functions is used with a cutoff of 400 eV to model the exchange and correlation functional [21]. The calculations have been carried out for three cases: (1) one oxygen (O) atom is substituted by a Vo ($Ti_{32}O_{63}$); (2) two O atoms are substituted by a Vo and a C atom ($Ti_{32}O_{62}C$); (3) a titanium (Ti) atom and two O atoms are substituted by an Fe atom, a V_O, and a C atom ($Ti_{31}FeO_{62}C$). The Monkhorst-Pack scheme k-points grid sampling was set to be 2 × 2 × 5 for the 95-atom anatase supercell. The valence electrons configurations for the O, C, Ti, and Fe are $2s^2\ 2p^4$, $2s^2\ 2p^2$, $3s^2\ 3p^6\ 3d^2\ 4s^2$, and $3d^3\ 4s^2$, respectively. All the atomic positions are fully optimized until the atom forces drop below the value 0.02 eV/Å.

3. Results and Discussions

Figure 1 exhibits the XRD patterns of the C doped TiO_2 films, C doped TiO_2 films (annealed in O_2), Fe-C codoped TiO_2 films, and Fe-C codoped TiO_2 films (annealed in O_2). It can be seen that the XRD diffraction peaks of the undoped TiO_2 film appearing around 25.3°, 36.9°, 37.8°, 38.5°, 48.0°, 53.9°, 55.0°, 62.1°, 62.6°, 68.7°, 70.2°, and 75.0° are indexed to (101), (103), (004), (112), (200), (105), (211), (213), (204), (116), (220), and (215) of the anatase phase (JCPDS, number 21-1272); and the XRD diffraction peaks at 26.7°, 34.0°, 51.7°, and 65.8° are

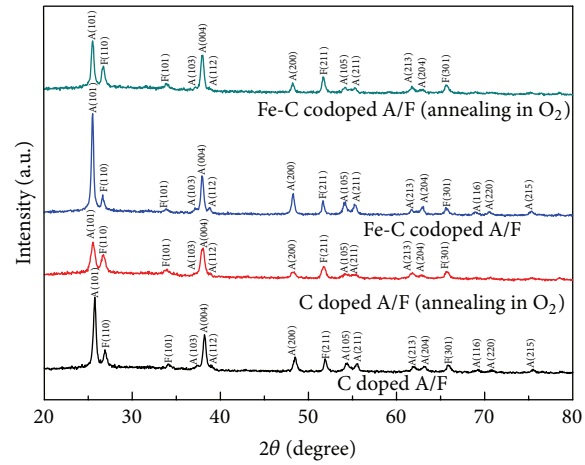

Figure 1: XRD patterns of the C doped A/F films, C doped A/F films (annealed in O_2), Fe-C codoped A/F films, and Fe-C codoped A/F films (annealed in O_2) on FTO substrates (A/F; A: anatase; F: ITO).

referred to as FTO (110), (101), (211), and (301). No signals of impurities such as rutile, $FeTiO_3$, or Fe cluster are detected. In addition, for the C doped TiO_2 films (annealed in O_2) and Fe-C codoped TiO_2 films (annealed in O_2), the XRD diffraction peaks show a relative lower intensity and a wider full width at half maximum (FWHM) comparing with the XRD data of C doped TiO_2 films and Fe-C codoped TiO_2 films. The average particle sizes of all the films were calculated and estimated using Scherrer equation choosing the Brag angle at (101), (004), and (200) diffraction peak. It is shown that the values of average particle size are 24.5 nm and 26.8 nm, for the C doped TiO_2 films and Fe-C codoped TiO_2 films, respectively. After the sample was annealed in O_2 gas, the values of average particle size decreased to 18.2 nm and 23.6 nm for the C doped TiO_2 films and Fe-C codoped TiO_2 films. The variation of the particle size originates from the difference of the doped element (Fe or C) and annealing gas (O_2).

Figure 2 demonstrates the XPS core levels for O-1s, C-1s, and Fe-2p of the Fe-C codoped TiO_2 films. As it is shown in Figure 2(a), the core level spectrum of O-1s is fitted with two peaks at 530.14 eV and 531.70 eV, attributed to O 1s in Ti-O linkages and Ti-O-C bonds of TiO_2, respectively. Figure 2(b) shows the core level spectrum of C-1s which can be fitted by four peaks at 284.84 eV, 286.71 eV, 283.6 eV, and 288.60 eV, respectively. The peak of 284.84 eV clearly arises from adventitious element carbon which also exists in the case of pure TiO_2 samples. The peaks at 286.71 eV, 283.6 eV, and 288.60 eV are attributed to C-O and C-Ti and COOH binding, respectively. Therefore, multiple carbon species, namely, substitutional and interstitial carbon atoms and carbonate species, coexist in the lattice of TiO_2. Figure 2(c) reveals the Fe 2p core level XPS spectrum. Apparently, there are two main peaks of Fe $2p_{3/2}$ and Fe $2p_{1/2}$ located at 710.71 eV and 724.52 eV, respectively, close to the binding energy of Fe^{3+} ion which indicates the existence of Fe^{3+} [22]. It is noticed that there is no weak peak at binding energy around 709 eV introduced by the contribution of Fe^{2+} ion in the spectrum.

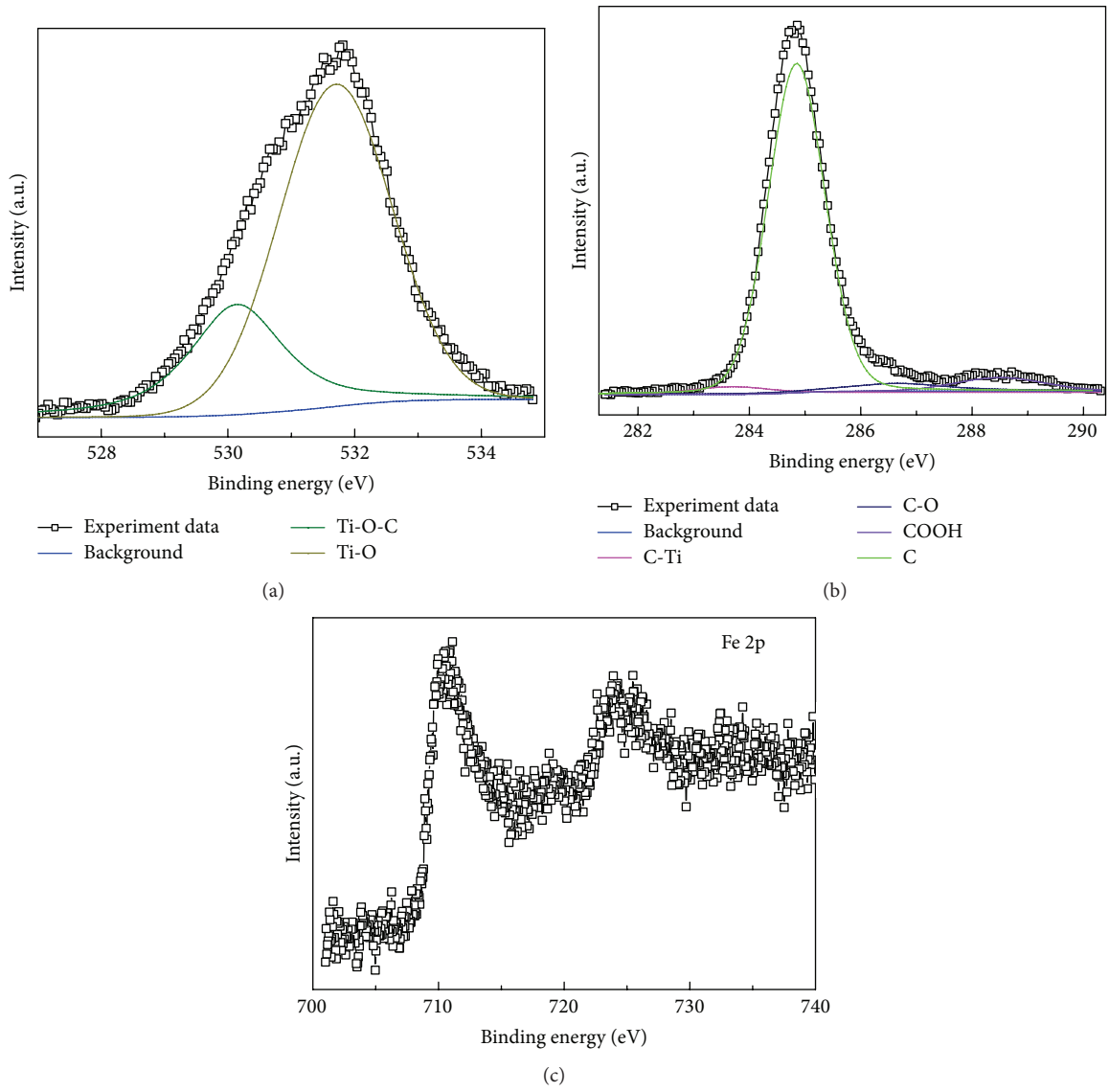

Figure 2: XPS of core level signals of (a) O1s, (b) C 1s, and (c) Fe 2p of the Fe-C codoped TiO_2.

Figure 3(a) illustrates the UV-Vis absorption spectra for these samples, which exhibit the characteristic spectrum of TiO_2 with its fundamental absorption edge around 384 nm (3.2 eV of band-gap energy). The absorption edges of the C doped TiO_2 films, C doped TiO_2 films (annealed in O_2), Fe-C codoped TiO_2 films, and Fe-C codoped TiO_2 films (annealed in O_2) are 387 nm, 370 nm, 399 nm, and 392 nm, with calculated band-gap energy of 3.20 eV, 3.35 eV, 3.11 eV, and 3.16 eV, respectively, similar to those reported in [23, 24]. Comparing with the samples annealed in O_2 atmosphere, the absorption edges of the C doped and Fe-C codoped TiO_2 films both shifted slightly toward the visible light range. The values of the band gap are in the following order: Fe-C codoped TiO_2 > Fe-C codoped TiO_2 (annealing in O_2) > C doped TiO_2 > C doped TiO_2 (annealing in O_2). The spectrum of Fe-C codoped sample yields the largest red shift which indicates the doping of Fe or C element may narrow the band gap.

Figure 3(b) presents the PL spectra of C doped TiO_2 films, C doped TiO_2 films (annealing in O_2), Fe-C codoped TiO_2 films, and Fe-C codoped TiO_2 films (annealing in O_2) at RT. The PL spectra are very sensitive to the stoichiometry and surface states for materials, which can provide information on electronic and optical properties [25, 26]. All the PL spectra of the specimens show two strong emission peaks at 468 nm and 480 nm, which are attributed to the Vos [27, 28]. The emission peaks corresponding to the defects are largely enhanced after annealing in O_2 gas.

Figure 4 shows the plots of magnetization (M) versus applied magnetic field (H) which demonstrate hysteresis behaviour in all samples measured by a VSM with the magnetic field from −1 to 1 T at RT. The values of the saturation magnetization (M_s) are in the following order: the C doped TiO_2 (annealed in O_2) < C doped TiO_2 < Fe-C codoped TiO_2 (annealed in O_2) < Fe-C codoped TiO_2.

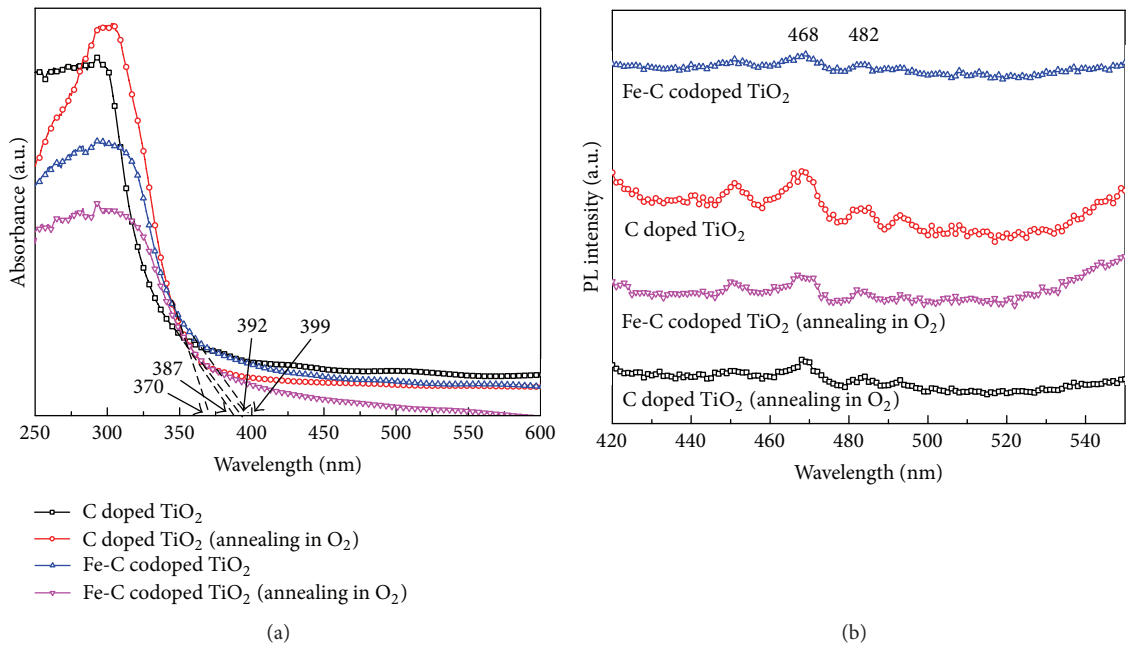

FIGURE 3: (a) The UV-Vis spectra and (b) PL spectra of the C doped TiO_2 films, C doped TiO_2 films (annealing in O_2), Fe-C codoped TiO_2 films, and Fe-C codoped TiO_2 films (annealing in O_2).

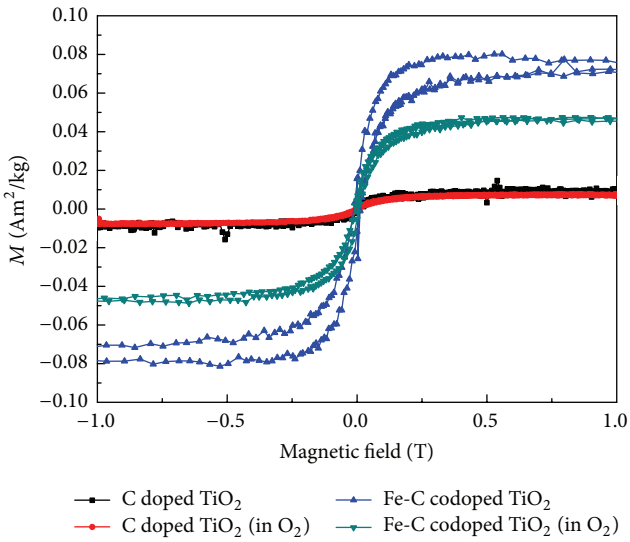

FIGURE 4: Hysteresis loops of the C doped TiO_2 films, C doped TiO_2 films (annealed in O_2), Fe-C codoped TiO_2 films, and Fe-C codoped TiO_2 films (annealed in O_2) at RT.

In order to understand the origin of RT FM in the Fe-C codoped TiO_2 films, the first-principles calculations are performed. The positions of V_O, Ti, Fe, C, and O for V_O-Fe-C codoped TiO_2 are the same as those of the V_O doped TiO_2 and the V_O-C codoped TiO_2. Firstly, when there exists only one Vo in the supercell, each Vo is assumed to donate two electrons. The result indicates that the two electrons created by one Vo are shared by three equivalent Ti^{3+} ions with up-spin of three different directions, which is similar to the results reported by Yang et al. [29]. The calculated net magnetic moment of the system is about 0.533 μ_B, which is related to the denoted two electrons that occupy the three neighboring Ti sites. The second and the third scenarios are V_O-C codoped TiO_2 ($Ti_{32}O_{62}C$) and V_O-Fe-C codoped TiO_2 ($Ti_{31}FeO_{62}C$), respectively.

Figure 5 shows the TDOS and PDOS of Vo-C codoped TiO_2 and Vo-Fe-C codoped TiO_2, respectively. The calculated band gaps using the GGA functional are about 2.09 eV for the Vo-C codoped TiO_2 and Vo-Fe-C codoped TiO_2, which is lower than the experimental value of 3.20 eV. However, the reduced band gap has nearly no influence on the magnetic state of C doped anatase TiO_2 and Fe-C codoped TiO_2.

Figure 5(a) shows the TDOS and PDOS of C 2p electrons for Vo-C codoped TiO_2 samples. It can be seen from Figure 5(a)I that there is no spin splitting around the Fermi level, which illustrates that the Vo-C codoped TiO_2 samples have no magnetic property. For the PDOS of C 2p electrons (in Figure 5(a)II) nearest to the Vo, there are also no exchange splitting around the Fermi level between the spin-up and spin-down states, lying within the band gap. With respect to the local Cartesian coordinate, the up-spin and down-spin of C $2p_x$, C $2p_y$, and C $2p_z$ states are all occupied. This indicates that the two electrons, created by one Vo, were trapped by the doped C atom. As a result, the valence electrons configuration for doped C atom is $1s^2\ 2p^6$, which produces 0 μ_B net magnetic moment.

Figure 5(b)I exhibits the TDOS for Vo-Fe-C codoped TiO_2 sample. It can be seen that a part splitting between the spin-up and spin-down states around the Fermi level is shown illustrating the existence of magnetism. For the PDOS of Fe 3d electrons (in Figure 5(b)II), the Fe 3d states are spin-polarized and lie within the band gap of Vo-Fe-C

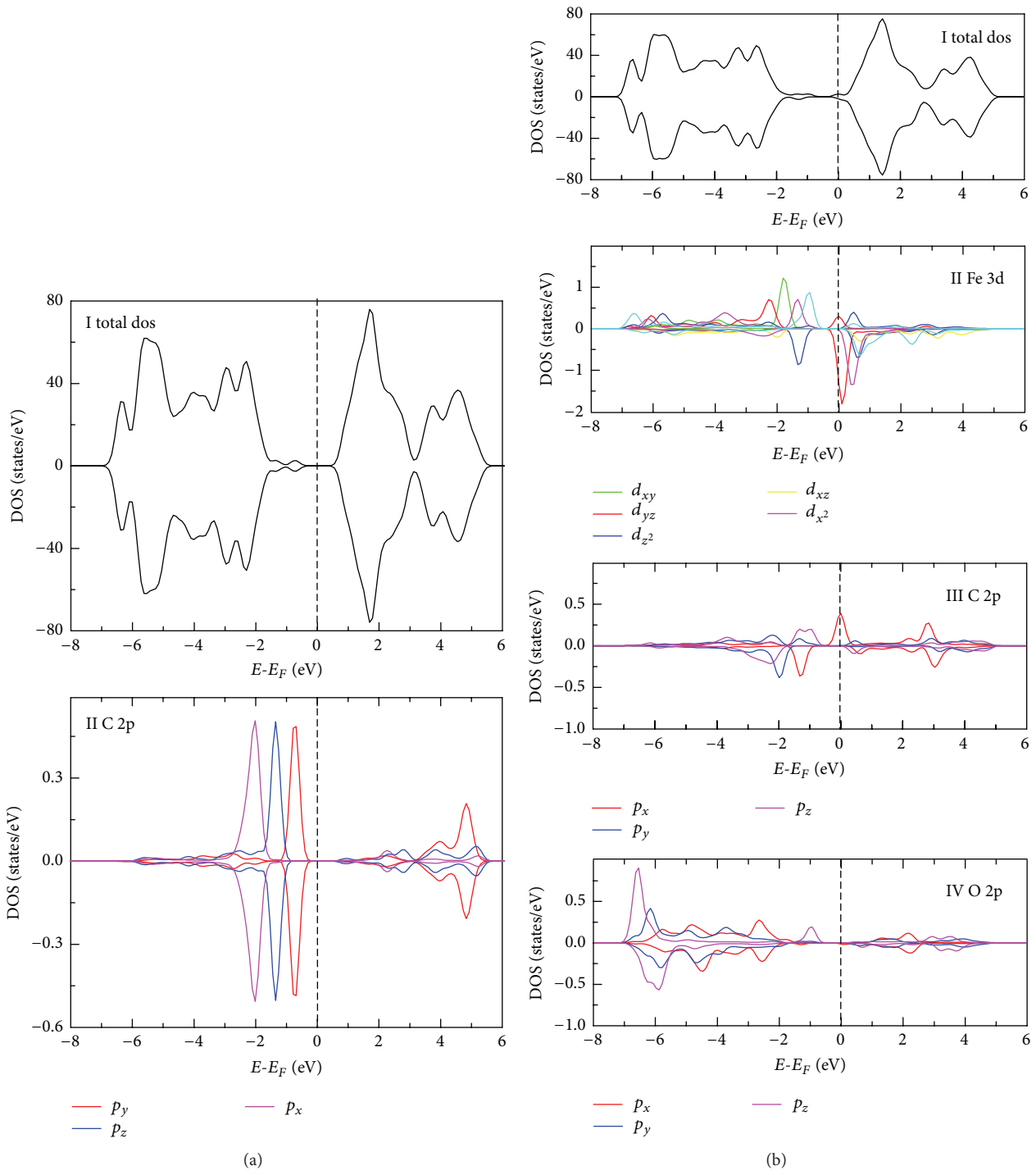

Figure 5: TDOS and PDOS for (a) V_O-C codoped TiO_2 and (b) V_O-Fe-C codoped TiO_2.

codoped TiO_2. With respect to the local Cartesian coordinate, the spin-up and spin-down states of Fe $3d_{yz}$ are occupied, while for Fe $3d_{xy}$, Fe $3d_{xz}$, and Fe $3d_{x^2}$ the spin-up states are occupied; for Fe $3d_{xy}$, only a few spin-down states are occupied. Noticeably, there are no spin-up and spin-down states of Fe $3d_{z^2}$ occupied. This indicates that each doped Fe atom at the Ti site produces the net magnetic moments of 2.538 μ_B, and its electron configuration can be resembled as Fe^{3+} ($3d^5$). For the PDOS of C 2p electrons (in Figure 5(b)III), the C 2p states are spin-polarized and lie within the band gap of Vo-Fe-C codoped TiO_2. With respect to the local Cartesian coordinate, the spin-up and spin-down states of C $2p_y$ and C $2p_z$ are all occupied, while, for C $2p_x$, the spin-down C $2p_x$ states are occupied and partly spin-up $2p_x$ states are not; as a result, the valence electrons configuration for the doped C atom is $1s^2$ $2p^5$. This indicates that each doped C atom at

the O site produces −0.025 μ_B net magnetic moments. For the PDOS of O 2p electrons (in Figure 5(b)IV), the C 2p states are partly spin-polarized and lie within the band gap of Vo-Fe-C codoped TiO_2. With respect to the local Cartesian coordinate, the spin-up and spin-down states of O $2p_x$, O $2p_y$, and C $2p_z$ are all occupied, but the slightly spin-up states of O $2p_z$ appear around Fermi level energy; as a result, the valence electrons configuration for O atom is $1s^2$ $2p^6$. The calculated net magnetic moment of O atom nearest to doped Fe atom is 0.075 μ_B.

To analyze the spin polarization induced by the doped Fe atom and C atom, we calculated the spin density distribution Fe and C atom. The calculated results are that the magnetic moment is mainly delocalized around the Fe atom, namely, about 2.538 μ_B on the Fe atom, about −0.025 μ_B on the C atom, about 0.079 μ_B on the nearest-neighbor O atom, and about 0.029 μ_B on the second-neighbor O atom. The calculated result indicates that the magnetic orbital describing the doped Fe, Vo, and C center extends to the second-nearest-neighbor O atoms. One of the two electrons created by the Vo is trapped by the doped C atom, and the other one is shared by Fe, C, and O atoms surrounding it. The total magnetic moment is 3.216 μ_B for the Vo-Fe-C codoped TiO_2.

Combining all the results presented above, we introduced a defect electron based model for the observed ferromagnetism. The magnetic moment is associated with a Vo, C^{2-}/Vo/Ti^{4+}, and C^{2-}/Fe^{3+}/Vo complex for Vo-C codoped TiO_2 and Vo-Fe-C codoped TiO_2, respectively. The magnetic orbitals extend to nearest neighbor and second neighbor around the complex. In the two models, the two electrons denoted by Vo mediate the coupling of C^{2-}/Vo/Ti^{4+} and C^{2-}/Fe^{3+}/Vo complex, possessing the characteristics of 3d electrons of Ti^{4+} and Fe^{3+}, occupying C 2p site, partly O 2p sites, and Fe^{3+} site. This is the original signal of the C^{2-} and Fe^{3+}, which also can be used to explain the reason that there is only Ti^{4+} signal appearing in XPS spectra. The value of total magnetic moment for Vo-Fe-C codoped TiO_2 and Vo-C doped TiO_2 is in the same order of M_s for Fe-C codoped TiO_2 and C doped TiO_2.

4. Conclusions

In summary, the RT FM properties of the C doped TiO_2 films and Fe-C codoped TiO_2 films have been investigated. The values of the saturation magnetizations are in the order of Fe-C codoped TiO_2 > Fe-C codoped TiO_2 (annealed in O_2) > C doped TiO_2 > C doped TiO_2 films (annealed in O_2). The calculated net moment values are in the order of Fe-C codoped TiO_2 > C doped TiO_2 with Vos existing, which are in accord with the experimental results. These calculations suggest the key factor for the formation of ferromagnetic ordering is the Vo which contributes two electrons to the doped C atom and neighboring O sites. The hybridization of Fe 3d, C 2p (nearest to the Fe atom), and O 2p (nearest to the Fe defect) led to the spin splitting of Fe 3d, C 2p, and O 2p which contributed to the magnetism. The unique characteristic of the defect electrons denoted by a Vo in Fe-C codoped TiO_2 and C doped TiO_2 is that they provide the means for the percolation of the magnetic complexes to achieve magnetization in the Fe-C codoped samples.

Competing Interests

The authors declare that there is no conflict of interests regarding the publication of this paper.

Acknowledgments

This work is supported by the NSFC nos. 11404100, 11175135, 10904116, and 11304083, the Key Scientific and Technological Project of Henan Province no. 102102210186, the Postdoctoral Research Foundation of Henan Normal University no. 01026500204, and the Scientific Research Foundation for Ph.D. of Henan Normal University nos. 01026500257 and 01026500121. This work is also supported by the High Performance Computing Center of Henan Normal University.

References

[1] B. Pal and P. K. Giri, "High temperature ferromagnetism and optical properties of Co doped ZnO nanoparticles," *Journal of Applied Physics*, vol. 108, no. 8, Article ID 084322, 2010.

[2] K. Ueda, H. Tabata, and T. Kawai, "Magnetic and electric properties of transition-metal-doped ZnO films," *Applied Physics Letters*, vol. 79, no. 7, pp. 988–990, 2001.

[3] X. Liu, J. Iqbal, Z. Wu, B. He, and R. Yu, "Structure and room-temperature ferromagnetism of Zn-doped SnO_2 nanorods prepared by solvothermal method," *The Journal of Physical Chemistry C*, vol. 114, no. 11, pp. 4790–4796, 2010.

[4] R. K. Singhal, A. Samariya, S. Kumar et al., "Study of defect-induced ferromagnetism in hydrogenated anatase TiO_2:Co," *Journal of Applied Physics*, vol. 107, no. 11, Article ID 113916, 2010.

[5] Y. Bai and Q. Chen, "First principle study of the cation vacancy in anatase TiO_2," *Physica Status Solidi—Rapid Research Letters*, vol. 2, no. 1, pp. 25–27, 2008.

[6] H. Peng, J. Li, S.-S. Li, and J.-B. Xia, "Possible origin of ferromagnetism in undoped anatase TiO_2," *Physical Review B—Condensed Matter and Materials Physics*, vol. 79, no. 9, Article ID 092411, 4 pages, 2009.

[7] N. Yu and J. W. Halley, "Electronic structure of point defects in rutile TiO_2," *Physical Review B*, vol. 51, no. 8, pp. 4768–4776, 1995.

[8] E. Cho, S. Han, H.-S. Ahn, K.-R. Lee, S. K. Kim, and C. S. Hwang, "First-principles study of point defects in rutile TiO_{2-x}," *Physical Review B*, vol. 73, no. 19, Article ID 193202, 2006.

[9] S.-G. Park, B. Magyari-Köpe, and Y. Nishi, "Electronic correlation effects in reduced rutile TiO_2 within the LDA + U method," *Physical Review B*, vol. 82, no. 11, Article ID 115109, 2010.

[10] M. Setvin, C. Franchini, X. Hao et al., "Direct view at excess electrons in TiO_2 rutile and anatase," *Physical Review Letters*, vol. 113, no. 8, Article ID 086402, 5 pages, 2014.

[11] M. Wang, M. Feng, and X. Zuo, "First principles study of the electronic structure and magnetism of oxygen-deficient anatase TiO_2 (0 0 1) surface," *Applied Surface Science*, vol. 292, no. 4, pp. 475–479, 2014.

[12] Z. Zhou, H. Wang, and Z. Yang, "Intrinsic defect-mediated magnetism in Fe-N codoped TiO_2," *Journal of Alloys and Compounds*, vol. 657, pp. 372–378, 2016.

[13] A. T. Brant, N. C. Giles, S. Yang et al., "Ground state of the singly ionized oxygen vacancy in rutile TiO_2," *Journal of Applied Physics*, vol. 114, no. 11, Article ID 113702, 2013.

[14] A. M. M. Navarro, C. E. R. Torres, V. Bilovol, A. F. Cabrera, L. A. Errico, and M. Weissmann, "Study of the relation between oxygen vacancies and ferromagnetism in Fe-doped TiO_2 nanopowders," *Journal of Applied Physics*, vol. 115, no. 22, Article ID 223908, 2014.

[15] B. Shao, Y.-F. He, M. Feng, Y. Lu, and X. Zuo, "Unexpected magnetic anisotropy induced by oxygen vacancy in anatase TiO_2: a first-principles study," *Journal of Applied Physics*, vol. 115, no. 17, Article ID 17A915, 2014.

[16] X. J. Wang, Y. L. Song, L. L. Tao et al., "Origin of ferromagnetism in aluminum-doped TiO_2 thin films: theory and experiments," *Applied Physics Letters*, vol. 105, no. 26, Article ID 262402, 2014.

[17] C. Lin, D. Shin, and A. A. Demkov, "Localized states induced by an oxygen vacancy in rutile TiO_2," *Journal of Applied Physics*, vol. 117, no. 22, Article ID 225703, 2015.

[18] R. Janisch, P. Gopal, and N. A. Spaldin, "Transition metal-doped TiO_2 and ZnO—present status of the field," *Journal of Physics: Condensed Matter*, vol. 17, no. 27, pp. R657–R689, 2005.

[19] G. Kresse and D. Joubert, "From ultrasoft pseudopotentials to the projector augmented-wave method," *Physical Review B*, vol. 59, no. 3, pp. 1758–1775, 1999.

[20] G. Kresse and J. Furthmüller, "Efficient iterative schemes for *ab initio* total-energy calculations using a plane-wave basis set," *Physical Review B-Condensed Matter and Materials Physics*, vol. 54, no. 16, pp. 11169–11186, 1996.

[21] J. P. Perdew, K. Burke, and M. Ernzerhof, "Generalized gradient approximation made simple," *Physical Review Letters*, vol. 77, no. 18, pp. 3865–3868, 1996.

[22] C. D. Wagner, W. M. Riggs, L. E. Davis, and J. F. Moulder, G.E. Muilenberg, editor, Perkin Elmer Corporation (Physical Electronics Division), Eden Prairie, Minn, USA, 1979.

[23] J. Yu, Q. Xiang, and M. Zhou, "Preparation, characterization and visible-light-driven photocatalytic activity of Fe-doped titania nanorods and first-principles study for electronic structures," *Applied Catalysis B: Environmental*, vol. 90, no. 3-4, pp. 595–602, 2009.

[24] W. Choi, A. Termin, and M. R. Hoffmann, "The role of metal-ion dopants in quantum-sized TiO_2: correlation between photoreactivity and charge-carrier recombination dynamics," *Journal of Physical Chemistry*, vol. 98, no. 51, pp. 13669–13679, 1994.

[25] Y. Lei, L. D. Zhang, G. W. Meng et al., "Preparation and photoluminescence of highly ordered TiO_2 nanowire arrays," *Applied Physics Letters*, vol. 78, no. 8, pp. 1125–1127, 2001.

[26] C. Huang, X. Liu, L. Kong, W. Lan, Q. Su, and Y. Wang, "The structural and magnetic properties of Co-doped titanate nanotubes synthesized under hydrothermal conditions," *Applied Physics A: Materials Science and Processing*, vol. 87, no. 4, pp. 781–786, 2007.

[27] J. H. Cho, B. Y. Kim, H. D. Kim et al., "Enhanced ferromagnetism in Co-doped TiO_2 powders," *Physica Status Solidi B: Basic Research*, vol. 241, no. 7, pp. 1537–1540, 2004.

[28] P. M. Kumar, S. Badrinarayanan, and M. Sastry, "Nanocrystalline TiO_2 studied by optical, FTIR and X-ray photoelectron spectroscopy: correlation to presence of surface states," *Thin Solid Films*, vol. 358, no. 1-2, pp. 122–130, 2000.

[29] K. Yang, Y. Dai, B. Huang, and Y. P. Feng, "Density-functional characterization of antiferromagnetism in oxygen-deficient anatase and rutile TiO_2," *Physical Review B-Condensed Matter and Materials Physics*, vol. 81, no. 3, Article ID 033202, 2010.